Weather and Climate Extremes 44 (2024) 100677

Contents lists available at ScienceDirect

Weather and Climate Extremes

journal homepage: www.elsevier.com/locate/wace

Amplification of the discrepancy between simplified and physics-based wet-bulb globe temperatures in a warmer climate

Liying Qiu [a,*], Ziwei Zhu [a], Zixuan Zhou [b], Eun-Soon Im [a,b,**], Seung-Ki Min [c,d,***], Yeon-Hee Kim [c], Yujin Kim [c], Dong-Hyun Cha [e], Joong-Bae Ahn [f], Young-Hwa Byun [g]

[a] Department of Civil and Environmental Engineering, The Hong Kong University of Science and Technology, Hong Kong SAR, China
[b] Division of Environment and Sustainability, The Hong Kong University of Science and Technology, Hong Kong SAR, China
[c] Division of Environmental Science and Engineering, Pohang University of Science and Technology, Pohang, South Korea
[d] Institute for Convergence Research and Education in Advanced Technology, Yonsei University, Seoul, South Korea
[e] Department of Civil, Urban, Earth, and Environmental Engineering, Ulsan National Institute of Science and Technology, Ulsan, South Korea
[f] Department of Atmospheric Sciences, Pusan National University, Busan, South Korea
[g] Climate Change Research Team, National Institute of Meteorological Science, Seogwipo, South Korea

ARTICLE INFO

Keywords:
Heat stress
Wet-bulb globe temperature
Climate change

ABSTRACT

The Simplified Wet Bulb Globe Temperature (sWBGT) is widely used in heat stress assessments for climate-change studies, but its limitations have not been thoroughly explored. Building on recent critiques of sWBGT's use for current climate on global scale, this study examines sWBGT's biases using dynamically-downscaled sub-daily climate projections under multiple future emission scenarios. The analysis is aimed at understanding caveats in the application of sWBGT and the uncertainties in existing climate change analysis dependent on sWBGT. Results indicate sWBGT's biases are heavily influenced by local near-surface air temperature, with overestimation of heat stress in East Asia regions, particularly hot and humid areas, due to static assumptions of radiation and wind speed. This overestimation is amplified in warmer climates, leading to exaggerated projected heat stress increases in future. In contrast, underestimations are found for heat stress levels attributed to low wind speeds and strong radiations, such as over the Tibetan Plateau and certain extreme events. Additionally, sWBGT underestimates variability in extreme heatwave events compared to WBGT in both current and future climates, irrespective of overestimation in absolute heatwave intensities. This study emphasizes the limitations of sWBGT, especially in future warmer climates. Importance of sub-daily data for capturing daily maximum heat stress level and reflecting diurnal variations in different components is also discussed. In conclusion, we recommend using Liljegren's model (i.e., physics-based calculation) with high-resolution sub-daily climate data for more accurate outdoor heat stress assessments in climate change studies.

1. Introduction

Wet-bulb globe temperature (WBGT) is a crucial index for assessing the level of human exposure to heat stress (Spangler et al., 2022). Compared to other heat stress indices depending solely on near-surface air temperature (TAS) and relative humidity (RH) (e.g., Apparent Temperature, Humidex, Wet-Bulb Temperature), WBGT is designed to additionally reflect the combined effect of wind and solar radiation (e.g., cloud cover and sun angle), taking into account various heat transfer processes on the human body in the outdoor environments. As a result, it is extensively adopted in various national (e.g., National Oceanic and Atmospheric Administration of US, Bureau of Meteorology of Australia) and international (e.g., the International Organization for Standardization) standards, particularly for assessing heat stress risk in outdoor workplace such as construction, agriculture, athletic, and military settings (Lemke and Kjellstrom, 2012).

However, WBGT observation is not commonly available due to the need for specialized equipment and expertise to measure. It is more

* Corresponding author. Department of Civil and Environmental Engineering, The Hong Kong University of Science and Technology, Clear Water Bay, Kowloon, Hong Kong SAR, China.
** Corresponding author. Academic Building 3594, The Hong Kong University of Science and Technology, Clear Water Bay, Kowloon, Hong Kong SAR, China.
*** Corresponding author. Division of Environmental Science and Engineering, Pohang University of Science and Technology, Pohang, South Korea
E-mail addresses: liying.qiu@connect.ust.hk (L. Qiu), ceim@ust.hk (E.-S. Im), skmin@postech.ac.kr (S.-K. Min).

https://doi.org/10.1016/j.wace.2024.100677
Received 29 May 2023; Received in revised form 22 January 2024; Accepted 3 May 2024
Available online 9 May 2024

often that WBGT is calculated using standard meteorological data obtained from observation or reanalysis (Spangler et al., 2022). The original outdoor WBGT (i.e., in the condition of direct sunshine) was constructed as a weighted average of the ambient temperature (T_a), the natural wet-bulb temperature (T_w), and the black globe temperature (T_g) (i.e., $WBGT = 0.1T_a + 0.7T_w + 0.2T_g$), and various methods have been developed to approximate it from the commonly available meteorological variables (e.g., TAS, RH, wind speed (WS), and surface downwelling shortwave radiation (RSDS)). According to Lemke and Kjellstrom (2012), more than seven calculation methods have been published to date, with Liljegren's model (Liljegren et al., 2008) considered the most accurate due to its solid physical basis and verification against observation (Kong et al., 2022; Lemke et al., 2012; Spangler et al., 2022). While the Liljegren's model has been used in the literature for reliable assessments of human heat stress (García-León et al., 2021; Grundstein et al., 2013; Spangler et al., 2022), the various simplified calculation methods (e.g., ACSM, 1984; Dunne et al., 2013; Lemke and Kjellstrom, 2012) continue to be widely adopted as proxies. Especially, one of the simplified versions of WBGT calculation, referred to as sWBGT hereafter (ACSM, 1984), appears to be dominantly employed in various studies, including but not limited to recent research in meteorology (e.g., Chen et al., 2020; Im et al., 2017; Lee and Min, 2018), economics (e.g., Liu et al., 2021; Parsons et al., 2022), agriculture (e.g., Lima et al., 2021), and public health (Urban et al., 2019). The simplicity of sWBGT calculation, which only requires TAS and RH, may explain its widespread use, but it is attention-worthy that the underlying bias behind such simplification is not fully discussed and often overlooked. This oversight may result in misleading results and interpretations among sWBGT users, which underscores the importance of clearer understanding in how the underlying assumptions of sWBGT might affect the conclusions drawn from its usage.

The bias in sWBGT arises from its assumption of a static outdoor environment with high solar radiation and low wind speed, disregarding their spatial and temporal variations. While Grundstein and Cooper (2018) compared sWBGT with Liljegren's approach using several station observations in the U.S., a recent study by Kong and Huber (2022), for the first time, explicitly explored the bias of sWBGT on a global scale and found that sWBGT overestimates heat stress in hot-humid areas but underestimating extreme heat in dry areas. However, as they focused solely on validating sWBGT in the current climate using reanalysis data, there is no clear explanation of how such bias translates into model projections aiming for climate change studies. Since sWBGT has been frequently used to assess future heat stress impacts under global warming, it is imperative to understand how the bias of sWBGT can impact the projected changes for evaluating its uncertainty and suitability for appropriate application.

Meanwhile, current heat stress impact studies mostly rely on daily meteorological data to calculate WBGT or sWBGT. Some studies simply used daily mean TAS and RH (e.g., Parsons et al., 2022), while others combined daily maximum TAS with daily mean (Lee and Min, 2018) or daily minimum RH (Russo et al., 2017) to approximate the daily maximum heat stress. However, there is no clarity on how well such approximations capture the daily extremes, whose accuracy may be predicated on the background climate, amplifying or dampening the actual maximum value. Besides the critical impacts of heat stress at the peak timing, it is also important to understand the characteristics of sub-daily WBGT, as it measures thermal comfort for guiding physical activities in an outdoor thermal environment that is directly impacted by a strong diurnal variation in meteorological variables (e.g., TAS, solar radiation). In fact, several studies have acknowledged the time-varying impacts of heat stress on human bodies and activities (e.g., labour loss, thermal disease), but the attempts for in-depth analysis of WBGT at a sub-daily time scale are relatively limited (Ullah et al., 2022) due to the rare availability of sub-daily climate data, particularly for long-term climate projections. Alternatively, statistical approaches, such as linear interpolation (Kjellstrom et al., 2018) or the statistical machine learning technique (Takakura et al., 2018), are sometimes utilized to approximate diurnal variation in WBGT using available daily data (e.g., daily mean TAS, daily maximum TAS). However, this may not be sufficient to reflect the synergistic effects of diurnal change in individual components of WBGT (i.e., T_a, T_w, T_g), which are influenced by a non-linear combination of four ambient factors (e.g., TAS, RH, radiation, WS). Moreover, this nonlinear relationship may exacerbate the discrepancy between WBGT and sWBGT in a non-uniform manner.

Given the aforementioned limitations, we recognize the necessity to conduct further investigation into the bias introduced by replacing explicitly-calculated WBGT (i.e., physics-based WBGT) with sWBGT, using high-resolution datasets. If the bias is systematic and significant, accurate projections of WBGT is required for updating the assessment of future heat stress in a rapidly warming climate. To address this issue, our study focuses on analyzing the discrepancy between sWBGT and WBGT not only in the present climate but also in future warmer climates under different warming scenarios. To achieve this, we utilize multiple climate projections over East Asia at a temporally and spatially fine-scale (3-hourly, 25 km), which were recently produced based on the dynamical downscaling of the UK Earth System Model (UKESM) in Coupled Model Intercomparison Project Phase 6 (CMIP6) using four Regional Climate Models (RCMs). With the updated projections generated within the state-of-the-art modeling framework, we provide, for the first time, the comparison of WBGT and sWBGT with an in-depth analysis of their characteristics under climate change over East Asia. The discrepancy between WBGT and sWBGT under various emission scenarios is discussed, including their abilities in describing heat stress levels and characterizing heatwave events for both current and future climates. This would provide valuable insights into how the bias in sWBGT behaves in response to different levels of warming and for different aspects of heat stress impact research.

2. Data and method

2.1. Data

In this study, two types of datasets are used: reanalysis and climate model projections. The reanalysis data from ECMWF-ERA5 (Hersbach et al., 2020) is used for analysing sWBGT bias in the present climate (1979–2014), and as a reference in the bias correction procedure. Climate projections are obtained from the outputs of four RCMs (Table S1) over the CORDEX-East Asia domain (Lee and Cha, 2020). They are the dynamical downscaling products of the UKESM in the newly released CMIP6. Four Shared Socioeconomic Pathways (SSPs) scenarios (i.e., SSP1-2.6, SSP2-4.5, SSP3-7.0, and SSP5-8.5) are included to cover low to high greenhouse gas emissions. The reference period is 1979–2014 (36-year) and the full future period is adopted till the end of the 21st century (2015–2 100), but the analysis is mainly focused on the last 36-year (2065–2 100).

For WBGT calculation, several variables are required, including 2-meter TAS, 2-meter RH, 10-meter WS, surface downwelling shortwave radiation (RSDS), and surface pressure. The variables at the same 3-hourly temporal frequency are extracted from all RCM simulations and ERA5. As RH is not directly provided in ERA5, near-surface dew point temperature is used together with TAS to derive RH by August–Roche–Magnus approximation. To ensure consistency, all RCM output is first spatially interpolated onto the $0.25^\circ \times 0.25^\circ$ regular latitude-longitude grid of ERA5 before conducting calculations and analyses. All calculation and analyses are conducted separately for each RCM first and the unweighted ensemble mean is presented.

2.2. Physics-based and simplified WBGT

As described above, the physics-based algorithm developed by Liljegren et al. (2008) is widely recognized as the most accurate way for

calculating WBGT. The algorithm is based on fundamental laws of mass and energy balance to describe physical processes on T_w and T_g sensors. The full descriptions and equations can be found in Liljegren et al. (2008) and are not detailed here. Liljegren et al. (2008) provided their original code, and we used here the code rewritten by Kong and Huber (2022) in Python.

sWBGT (ACSM, 1984) is designed to approximate outdoor WBGT as a function of TAS and RH (Eq. (1)), assuming constant moderate solar radiation and relatively low WS.

$$sWBGT = 0.567TAS + 0.393e + 3.94 \quad (1)$$

Where e is the vapor pressure (hPa) calculated as

$$e = \left(\frac{RH}{100}\right) \times 6.105 \times exp\left(\frac{17.27TAS}{237.7 + TAS}\right) \quad (2)$$

In this study, we treat WBGT calculated from Liljegren's model as the reference standard to measure the bias brought by the simplified calculation. WBGT and sWBGT stand for the physics-based and simplified calculation, respectively. The bias of sWBGT is defined as the discrepancy of sWBGT from WBGT (bias = sWBGT − WBGT).

2.3. Bias correction

As climate models are unavoidably prone to biases from various sources, bias correction is applied to correct the calculated heat stress indices from climate projections. Specifically, the trend-preserving method of Quantile Delta Mapping (QDM) is directly applied to the WBGT and sWBGT after they are calculated from the original meteorological variables. We proved this bias correction strategy, in a previous study using the same RCM data as in this study (Qiu et al., 2023), as an appropriate approach for adjusting heat stress projections.

QDM is applied in 36-year sliding windows with a 12-year interval. Replacing the central 12 years, each 36-year window slides forward 12 years until the end of the projection. To maintain the diurnal and interannual cycle, bias correction with the sliding window is applied separately for each 3-h interval in each calendar month (e.g., June 00UTC).

2.4. Analysis of heatwave characteristics

For characterizing heat stress, we narrow our focus to the summer season (June-July-August: JJA) and over land points. After calculating and bias-correcting 3-hourly WBGT/sWBGT, the data is converted to the local time zone of each grid cell using the "lutz" R package (Spangler et al., 2022). The daily maximum and daily minimum values are picked up and labeled as WBGTmax/sWBGTmax and WBGTmin/sWBGTmin, respectively.

In addition to the statistics of daily WBGTmax/sWBGTmax, we also analyze the characteristics of heatwave events based on consecutive days exceeding a certain threshold. In this study, a heatwave event is defined as a period of at least three consecutive days, a commonly adopted criterion in the literature (Becker et al., 2022; Chen et al., 2020; Li, 2020), during which WBGTmax/sWBGTmax exceeds the chosen threshold. The threshold is the local 99th percentile (Bumbaco et al., 2013; Chen et al., 2020; Hajat et al., 2002) during the respective periods. Instead of taking the same threshold for the current and future climates, we adopt the period-based thresholds for counting the extremes in the corresponding periods. This method is for focusing on different behaviors of heatwaves emerging under a new "norm" of a warmer climate, by minimizing the effect of the increase in mean TAS itself. For each heatwave event, the mean intensity (mean WBGTmax/sWBGTmax during the heatwave event) and mean relative intensity (relative intensity = intensity – threshold) are counted. While the mean intensity indicates the severity of heatwave events, the relative intensity can provide clues about the local variability of how far the events deviate from the threshold.

It is noteworthy that although heatwaves are commonly recognized as periods of abnormally hot weather, there is no universal definition for it (Perkins, 2015; Sulikowska and Wypych, 2020), which instead naturally varies based on the objectives of different studies, such as assessing the heatwaves' impacts on health, ecosystems, or infrastructures. While we apply a heatwave definition of WBGTmax exceeding local 99th percentile for at least three consecutive days in this study, sensitivity tests using different numbers of consecutive days (i.e., four and five), and why using the absolute thresholds for heatwave (such as >35 °C) is inappropriate for this study, are discussed in Section 3.3. We also note that the majority of computed WBGTmax/sWBGTmax values fall into the range of 25–35 °C (Figs. S1 and S2), which indicates that they are within the range of potential outdoor heat injury, and thus worth investigating. Although the WBGT/sWBGT levels in Tibet (TBT) may indicate low absolute risk for heat injury, it is still valuable for analysis because the sensitivity of heat injury to heat stress indices may vary among regions and populations, so we do not artificially remove any locations upon the predefined threshold.

3. Results

3.1. The discrepancy between sWBGT and WBGT in the present climate

Taking WBGTmax computed by the Liljegren's model as the ground truth, Fig. 1 illustrates the spatial distribution of the bias in sWBGTmax relative to WBGTmax during the historical period, averaged over the 36 years of JJA mean and maximum. The QDM corrected model output well follows the reanalysis data. As shown in Fig. 1a–c, a consistent overestimation in mean sWBGTmax is visible across the study domain, except for the TBT. The mean sWBGTmax overestimation is greater in hot, humid regions such as India, Southeast Asia, and South China, while it is lower in higher latitudes. Fig. 2 displays the diurnal cycles of both the heat stress indices and their components averaged over regions classified by their mean sWBGTmax bias, excluding areas with negligible bias (i.e., −0.5 °C < bias<0.5 °C). R1 is a region showing underestimation in the sWBGTmax (bias < −0.5 °C), which is opposite to the majority of regions in the study domain. The negative bias mainly occurs around the TBT region, where the simplified calculation reflects only the relatively low TAS and low RH during the daytime but neglects the local high peak of radiation. On the other hand, R2, mostly located north of 30°N, exhibits the least bias, as it comprises the temperate climate zone that generally meets the sWBGT's assumption of "moderate solar radiation and relatively low WS". R3 and R4 are regions with relatively high overestimation in the daily maximum. It is evident that these regions have relatively high TAS, RH, and WS (i.e., coastal regions with hot, humid climates). Without considering the high WS, sWBGT building on the high TAS and RH shows a clear overestimation, and the warm bias is larger in the region with higher TAS (i.e., R4). The assumption of constant outdoor radiation and wind speed in sWBGT makes it suitable for estimating WBGTmax only over very limited regions, and there is a clear regional variation in the sWBGT bias relevant to the local climate characteristics. However, despite the spatial variation of bias in the daily maximum, the bias of sWBGT in terms of the daily minimum (i.e., sWBGTmin) is rather homogenous across the domain (low CV value) with an evident overestimation (Fig. S3). Given sWBGT's underlying assumptions of radiation, it is not appropriate for assessing heat stress during the nighttime under any circumstance and thus leads to such overestimations in the daily minimum.

Interestingly, the overwhelming overestimation is not observed in the extremes (i.e., JJA maximum). The 36-year averaged bias of the JJA maximum is displayed in Fig. 1b–d. The warm bias is reduced and even reversed to a cold bias, with a greater underestimation over TBT. Fig. S4 shows the spatial patterns of TAS, RH, RSDS, and WS averaged over the timing when sWBGTmax and WBGTmax reach their seasonal maximums on each grid point, respectively, while Fig. S5 shows the average

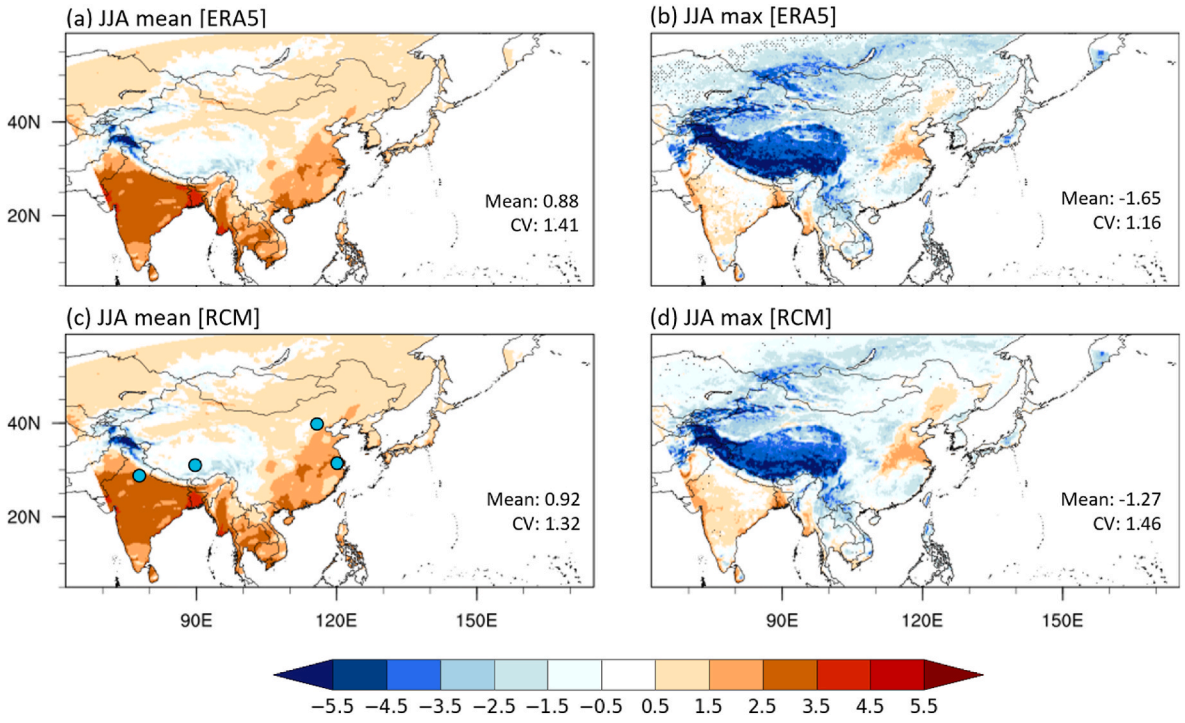

Fig. 1. The spatial distribution of bias in sWBGTmax (i.e., sWBGTmax – WBGTmax) in terms of the 36-year average of JJA (a, c) mean and (b, d) maximum. The data is from (a, b) ERA5 and (c, d) the ensemble mean of four RCMs' QDM-corrected output during historical period (1979–2014). The black dotted areas are with less than 75% of years agreeing with the sign. The four blue circles on (c) are the locations of the grid points selected as representative of Lhasa (29.75°N, 91.25°E), Shanghai (31.25°N, 121.50°E), New Delhi (28.50°N, 77.25°E), and Beijing (40.00 °N, 116.50°E) for the analysis in Section 3.2 and 3.3. The unit is °C. The spatial mean and coefficient of variation (CV = Standard Deviation/mean) over the region are marked on each sub-figure. (For interpretation of the references to color in this figure legend, the reader is referred to the Web version of this article.)

throughout the whole summer. It can be seen that when WBGT reaches extremes, not only is TAS high, but high RSDS and very low WS are consistently observed across the entire domain. In comparison, sWBGT simply reflects its extremes based on the high TAS. However, it falls short in accurately measuring the intensity of extreme conditions and overlooks the precise timing of heat extremes that signal a higher likelihood of heat injury for individuals exposed to outdoor heat stress, which is captured by WBGT. In this regard, sWBGT may not be effective and may not offer significant advantages over heat stress indicators based solely on TAS and RH in guiding outdoor activities.

On the other hand, given that many previous studies used daily meteorological data for deriving daily WBGTmax/sWBGTmax, we calculate the average hour of the day when each component reaches their maximum (minimum for RH) to check if daily data can well capture the diurnal peak of the heat stress (Fig. 3). Our findings show that for sWBGT, the timing of daily maximum TAS and daily minimum RH are highly similar, resulting in sWBGT also peaking around the same time. In contrast, for WBGT, its component—radiation (i.e., RSDS)—usually reaches its maximum earlier in the day than TAS, leading to an "intermediate" pattern in the peaking timing between maximum TAS and RSDS. The diurnal variation of WS may not significantly affect the peak time of WBGT as it is usually smaller than that of the other components (Fig. 2). This result suggests that sub-daily meteorological data is necessary not only for capturing sub-daily variations in heat stress but also for more accurate calculation of the daily maximum due to the lag among the diurnal cycle of the components. Furthermore, without taking radiation effect into consideration, sWBGT cannot accurately reflect the diurnal cycle of heat stress even using the sub-daily data.

3.2. *The discrepancy between sWBGT and WBGT in the future warmer climate*

In this section, we investigate the bias of sWBGT in projecting changes in heat stress under global warming. Fig. 4 shows the spatial distribution of bias at the end of the 21st century for the projected change in summer mean and maximum sWBGTmax. Overestimation in the change of mean is primarily observed in south and southeast Asia, and Eastern China, with other regions showing minimal bias. The degree of bias is scaled with the emission scenarios, with the largest found in SSP5-8.5 and the least in SSP1-2.6. A larger overestimation is identified in the extremes (i.e., JJA max) across most regions, except for TBT, although the spatial distribution remains similar to that of the mean.

To understand the dependencies of bias in projected heat stress change on different ambient factors, Fig. 5 presents a schematic figure illustrating how the bias of projected change of sWBGT varies as each component variable changes (i.e., ΔTAS, ΔRH, ΔRSDS, and ΔWS). Here, "Δ" denotes the change between the future and historical periods of the variable. The values (on the upper left legends) are selected to qualitatively represent the possible variations of the meteorological variables over the study domain considering both mean and extreme cases (spatial quartiles are marked on Figs. S4–S5). In Fig. 5a, it is clear that the overestimation in sWBGT's projected change (i.e., Δ sWBGT – ΔWBGT) increases as both the background TAS (i.e., historical TAS) and the TAS change (i.e., ΔTAS) increase. This implies that even under the same degree of warming, a larger overestimation in heat stress will be found for a place with a hotter climate condition when projected using sWBGT. A similar pattern is found in RH, in which both the background humidity and humidity increase result in a larger overestimation. Note that when RH is relatively low (e.g., RH = 30%), sWBGT might underestimate heat stress under certain conditions, such as low wind and high radiation. The same applies when RH decreases in the future, where sWBGT

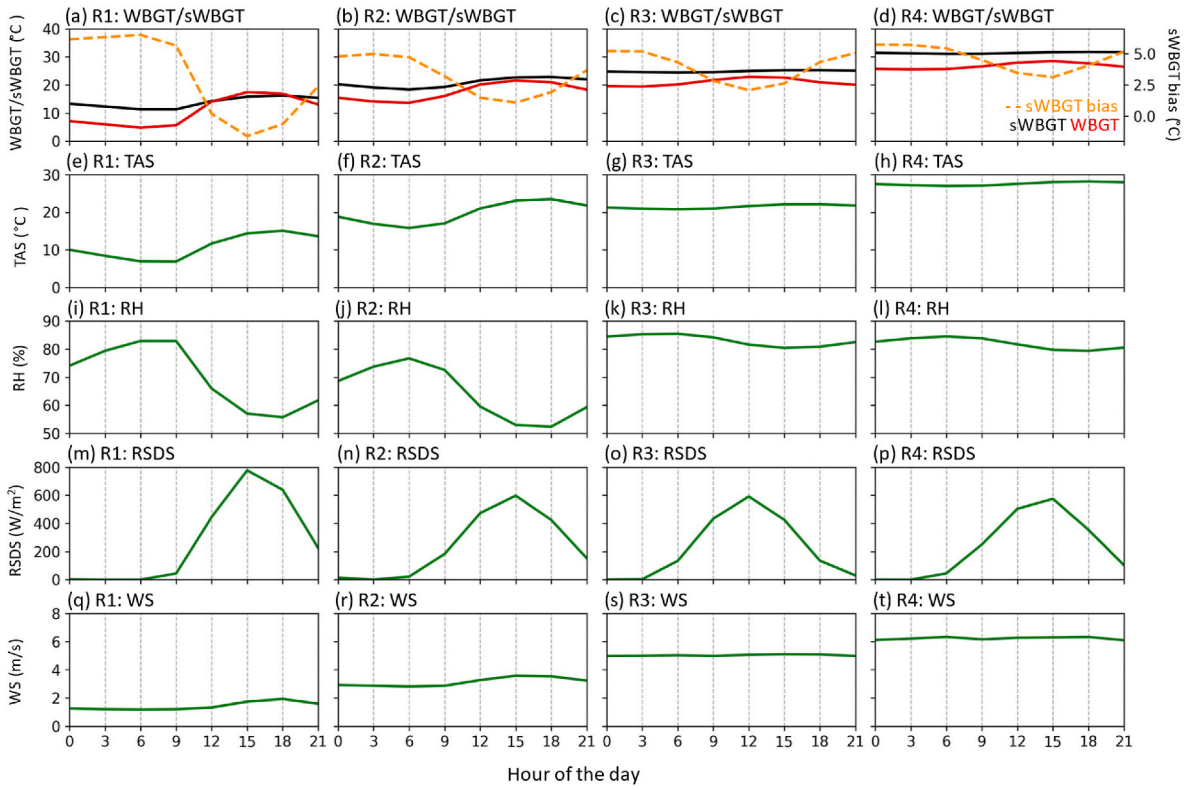

Fig. 2. The diurnal cycle of (a–d) sWBGT (black) and WBGT (red), (e–h) TAS, (i–l) RH, (m–p) RSDS, and (q–t) WS averaged over areas with mean sWBGT bias, as shown in Fig. 1a, in the range of < -0.5 °C (first column, R1), 0.5–1.5 °C (second column, R2), 1.5–2.5 °C (third column, R3), and >2.5 °C (fourth column, R3), during JJA, historical period in ERA5 reanalysis data. (For interpretation of the references to color in this figure legend, the reader is referred to the Web version of this article.)

underestimates the effect of reduced RH.

On the other hand, the change of WS affects the bias in ΔsWBGT significantly under conditions of low background WS (e.g., 0.5 m/s), compared to higher background WS (e.g., 2.5 m/s or 4.5 m/s). As extremely low wind speeds are observed during the events when WBGT reaches its high extremes, in contrast to the extremes of sWBGT (Fig. S4 d and h), sWBGT may underestimate the effect of WS changes on the projection of heat stress. It should be noted that the bias in ΔsWBGT discussed here differs from the bias in sWBGT discussed in the previous section. For example, sWBGT is likely to overestimate more for a higher historical WS; however, such bias is more likely to remain stable when WS continues to increase in the future, compared to a case with a lower historical WS. Therefore, the difference of bias between the future and historical periods is less significant. The same applies to RSDS, where a smaller bias of ΔsWBGT is observed in higher background RSDS. However, such a bias is not linearly scaled by either background RSDS or ΔRSDS, that in Fig. 5d the lines of background RSDS at 450W/m^2 and 650W/m^2 show little difference until the ΔRSDS reaches +25W/m^2. Furthermore, unlike other factors showing overestimated ΔsWBGT with the increase, sWBGT will underestimate the heat stress level increase when RSDS increases, as the simplified assumption cannot reflect the thermal heating effects from increased radiation.

In Fig. 6, we choose four city points from Lhasa (29.75°N, 91.25°E), Shanghai (31.25°N, 121.50°E), New Delhi (28.50°N, 77.25°E), and Beijing (40.00 °N, 116.50°E), respectively, to illustrate how the bias of sWBGT varies in response to different ambient environments and levels of warming. While Shanghai, New Delhi, Beijing are densely populated cities within the study domain where the populations are likely to witness heat injuries during the heatwaves, Lhasa is selected as another example due to its contrasting bias signal (i.e., the underestimation of bias over TBT), which has not been well discussed in previous literatures and thus is worth investigation. Also, it should be noted that even though the sWBGT/WBGT levels seem not to constitute huge risks of heat injury, heat stress is not entirely negligible in TBT (Bai et al., 2016; Wei et al., 2023). In fact, the sensitivity of heat injury to heat stress index levels varies among regions and populations, therefore it is still important to understand their change for different regions.

The contour shading in Fig. 6 reflects the bias of sWBGT across ranges of TAS and RH, with the difference in shading determined only by WS and RSDS levels in WBGT calculation, as noted on the subtitles. The WS and RSDS are approximated by the mean and the extreme (when sWBGTmax/WBGTmax reach their JJA maximums) cases respectively. The dots on Fig. 6a–d represent the days when WBGT reaches the 0-100th percentiles in the current and future (SSP5-8.5) climates, while Fig. 6e–h compare only the 100th (i.e., the maximum) percentile from different emission scenarios. Based on the mean state, the positive bias is more pronounced under future warming scenario (i.e., SSP5-8.5), and is exacerbated by concurrent hot (i.e., high TAS) and humid conditions. For instance, while both Shanghai and Beijing experience comparable TAS, Shanghai exhibits a greater positive bias attributed to higher levels of humidity. In comparison, although New Delhi and Beijing are differently located in space, they exhibit similar bias patterns, possibly due to similar TAS and RH. As for the extreme cases, it turns out that WS and RSDS can critically affect the sign of sWBGT bias. In other words, negative biases (sWBGT < WBGT) may occur under strong solar radiation and light wind conditions. For a relative cold and dry region (e.g., Lhasa), such effects lead to a significant underestimation in the extreme heat stresses for both current and future climates. Nevertheless, given any fixed level of WS and RSDS, larger positive biases tend to occur under hotter and more humid conditions. This explains the positive bias in the extremes over Shanghai (in YRD) as well as the overestimation in the projected change of heat stress in Fig. 4.

Although the changes of four ambient factors all influence the bias of sWBGT, TAS clearly shows the largest impact, and the bias magnitude

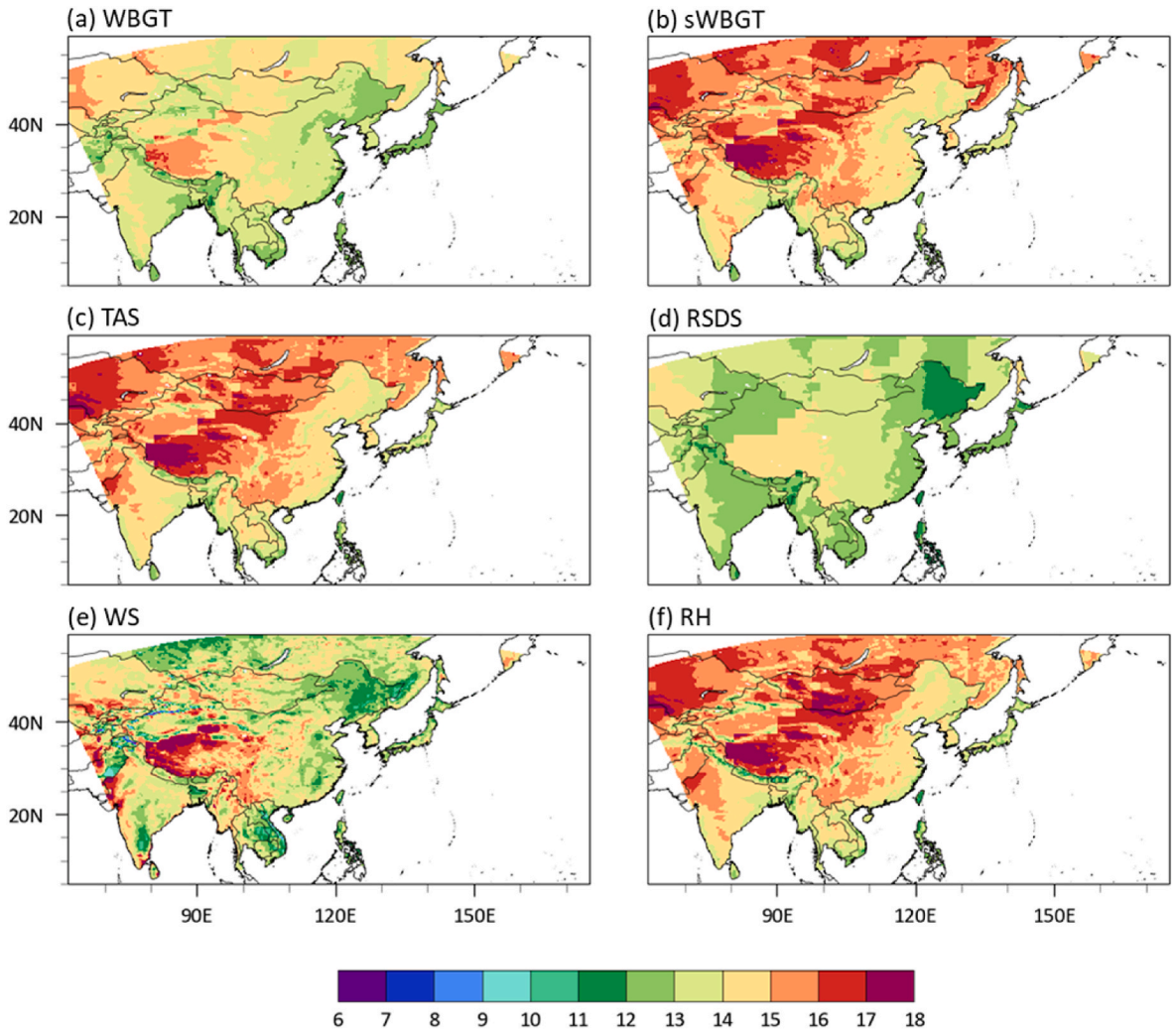

Fig. 3. The average hour of the day when (a) WBGT, (b) sWBGT, (c) TAS, (d) RSDS, (e) WS reach their daily maximum, and when (f) RH reaches its daily minimum during JJA, historical period in ERA5 reanalysis data. The time has been adjusted to local time zone.

significantly increases as TAS rises, which therefore further impact the bias of projected change. Meanwhile, as the spatial variation of ΔTAS (i.e., warming degree) is smaller compared to that of the climatological TAS pattern (Figs. S6 and S7), the pattern of climatological TAS mostly determines the spatial pattern of the bias in ΔsWBGT (Table 1), while the ΔsWBGT and ΔWBGT themselves follow the pattern of ΔTAS (Tables S2 and S3). Again, we emphasize that the bias in the climatological sWBGT and the bias in ΔsWBGT are determined by different factors non-linearly, as previously illustrated. While the underestimation in climatological sWBGT extremes is due to a systematic ignoration of high radiation and low wind cases, the overestimation of the change in sWBGT extremes is scaled mostly by the corresponding TAS.

3.3. The discrepancy between sWBGT and WBGT in describing heatwave characteristics

Defined in Section 2.4, the mean intensity and relative intensity of heatwaves in the historical and future, taking SSP5-8.5 as an example, are displayed in Figs. 7 and 8, respectively. Unsurprisingly, Fig. 7 reveals amplified heatwave intensities in the future relative to the historical period, as projected by both WBGT and sWBGT. This is mainly due to the increased thresholds (i.e., the 99th percentile of the period), along with the elevated mean TAS, in future periods, resulting in higher intensity levels of the considered heatwaves. In this context, the bias of sWBGT, in each period, shows a spatial distribution "intermediate" between that of the mean and that of the maximum (Fig. 1c and d). Consistent with prior findings presented in Fig. 4, overestimation is also found for the projected heatwave intensity increase in sWBGT, resulting from the amplified overestimation in a warmer climate.

By removing the local period-based percentile thresholds, the relative intensity in Fig. 8 focuses more on the variability of local "hot days" rather than variation among different regions or between the periods. Consequently, much less spatial variation (less than 1 °C across the study region) and future changes (less than 0.5 °C for SSP585) are found. However, concerning sWBGT bias, a clear underestimation is observed across the study region. It starkly contrasts the aforementioned pattern of bias in both mean heat stress levels and the absolute intensities of heatwave events. This might be explained by a decreased variability characterized by sWBGT when compared to the full version. In Fig. 9, the kernel density distributions of heat stress levels during the heatwave events (sWBGTmax/WBGTmax during the heatwave events pooled together from all the days) from Lhasa, Shanghai, Beijing, and New Delhi are used to display the variability in extreme heat stress levels. A "taller" peak in the distribution of the extreme sWBGT than the WBGT suggests an underestimation of heatwave variabilities, resulting in a lower relative intensity as shown in Fig. 8. Such variabilities comprise both interannual and day-to-day variations in the daily maximum heat stress levels. The negative bias for the range in the annual mean heatwave intensities shown in Fig. S8 is a demonstration for the underestimated interannual variability in sWBGT.

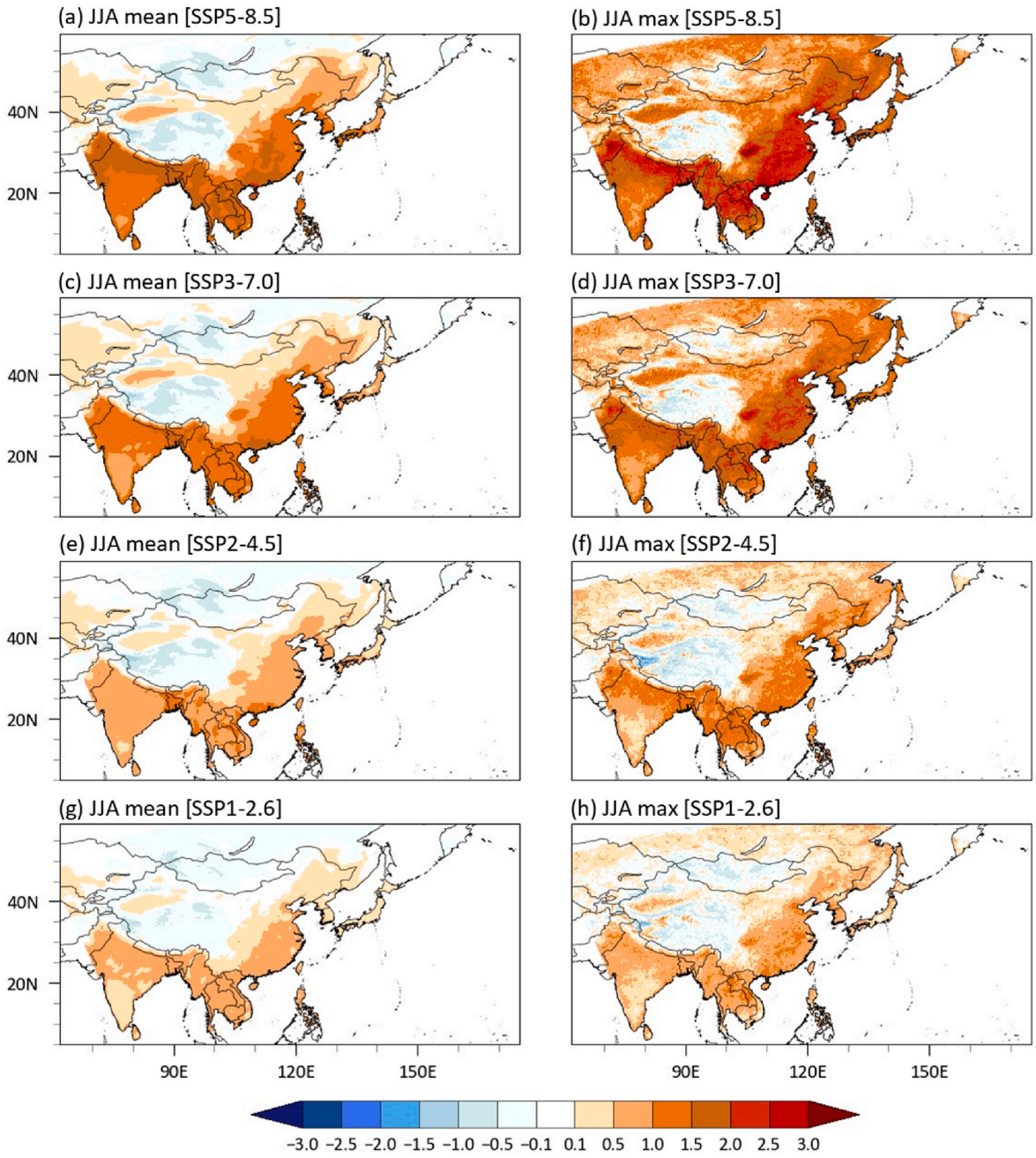

Fig. 4. The spatial distribution of bias in sWBGTmax in terms of the projected change (2065–2100 vs. 1979–2014) of (a, c, e, g) the mean and (b, d, f, h) maximum of the WBGTmax under four SSP emission scenarios from the ensemble mean of four RCMs' QDM-corrected output during JJA. The unit is °C.

As previously indicated in Section 2.4, while there is no universal definition of an heatwave event, we employ period-based percentiles as the heatwave threshold in this study to highlight heatwave characteristics under a new "norm" (i.e., a higher mean TAS) for examining discrepancies between sWBGT and WBGT in describing heatwave features. Compared to historical-percentile (e.g., Bumbaco et al., 2013; Chen et al., 2020; Hajat et al., 2002) or region-specific absolute thresholds (e.g., Hayhoe et al., 2004; Kim et al., 2016; Mcurari et al., 2015), the change of period-based threshold is less affected by the dominant effect of mean TAS increase. In addition, since we focus on a large domain, and solely during the summer season, using percentile-based threshold will ensure the consistency of our standards over different sub-domains with discrepant background climates.

Nevertheless, we understand that heatwave assessment results could be sensitive to various definitions (Xu et al., 2016). Therefore, sensitivity tests have been conducted for exceeding the local 99th percentile threshold for different numbers of consecutive days (i.e., four and five; Figs. S9 and S10). The results show that changing the number of consecutive days produces no significant differences in the heatwave characteristics, thereby fortifying the robustness of our findings. However, applying an absolute threshold, usually based empirically on heat exposure research, on sWBGT may lead to further biased results considering the systematic overestimation in it. This also hinders a comparison of the derived heatwave event with those derived using WBGT, making it less suitable for our study. Note that although the heat stress levels derived over the TBT region might correspond to an absolute value too low to have adverse impacts, we apply the period-based 99th percentile threshold to TBT region, instead of absolute thresholds, to avoid artificially removing any data points and provide a more holistic picture of heat stress changes by including its contrasting

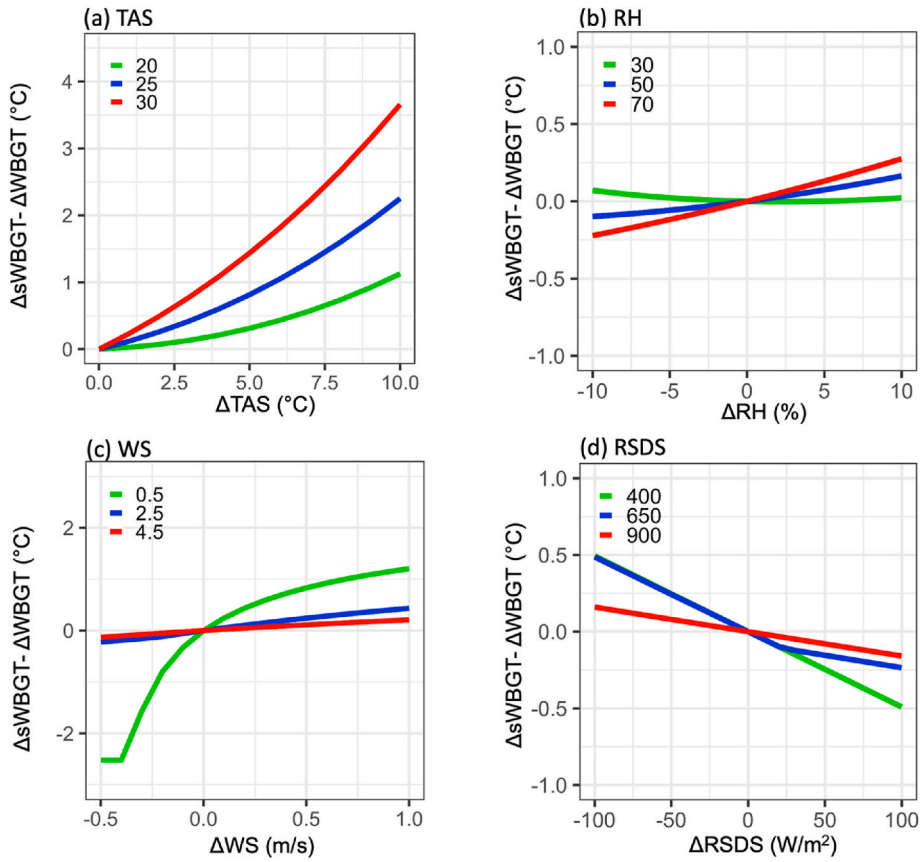

Fig. 5. The schematic figure of how the bias of projected sWBGT change (y axis) evolves against the change (x axis) in (a) TAS, (b) RH, (c) WS, and (d) RSDS. In each sub-figure, the colors of the lines stand for different background conditions of the varying variables, and we assume the other variables as statically moderate situation (i.e., TAS = 25 °C, RH = 50%, WS = 2.5 m/s, RSDS = 650W/m^2). The units for WBGT/sWBGT/TAS are °C, for RH is %, for RSDS is W/m^2, and for WS is m/s. (For interpretation of the references to color in this figure legend, the reader is referred to the Web version of this article.)

behavior compared to other regions.

4. Discussion and conclusion

sWBGT has been widely used in various heat stress impact assessments due to its simplicity in calculation. While recent studies have criticized sWBGT for its inaccuracies (e.g., Kong and Huber, 2022), they focus solely on current climate using reanalysis data may not be sufficient in understanding the implications for future climate projections. Therefore, our research expands upon this by providing a comprehensive investigation of sWBGT's biases in both current and future climates, based on the assumption that the WBGT computed through Liljegren's model is the ground truth. The term "bias" refers to the gap of sWBGT from Liljegren's WBGT, whereas the word 'difference' is exclusively used for describing a different behavior of the 'bias' (i.e., discrepancies in the bias amount). The study is expected to enhance the understanding of sWBGT's limitations and offer insights into the uncertainties lying in the existing heat stress assessments that is dependent on sWBGT.

Our findings indicate that the bias of sWBGT, in both current and future climates, is strongly influenced by local climate characteristics. In most regions of East Asia, sWBGT overestimates heat stress levels, with the bias being more pronounced in hot and humid regions. Especially, when TAS reaches over 40 °C, which is more likely to happen as climate warms, the overestimation reaches over 8 °C for the humid regions (Fig. 6). Likewise, sWBGT overestimates the increase in heat stress levels as TAS rises in the future projections, with the degree of overestimation highly correlated with local climatological TAS. In the meantime, due to the lag among the diurnal cycles of the relevant variables (i.e., TAS, RH, RSDS), sub-daily meteorological data is necessary for accurately capturing diurnal variations and daily maximums when calculating the outdoor heat stress.

Conversely, in certain regions and under specific conditions, sWBGT also underestimates heat stress levels. The cold-dry, plateau area of Tibet serves as an example, where sWBGT fails to account for the significant diurnal variation in solar radiation. Similarly, extreme heat stress events are often associated with strong radiation and low wind, leading sWBGT to underestimate these occurrences and intensities given its static assumption in these two ambient factors.

When comparing sWBGT and WBGT for heatwave analysis, we find a surprising underestimation of relative heatwave intensity in sWBGT. This underestimation is in contrast to the overestimation observed in mean heat stress levels and absolute heatwave intensity. It demonstrates the sWBGT's inability to accurately capture the variability among extreme events, regardless of their absolute magnitudes.

Among the existing literature, many studies employing sWBGT suggested more intense, prolonged, and frequent heatwaves under future climate change scenarios (e.g., Chen et al., 2020; Im et al., 2017; Lee and Min, 2018), which leads to heightened risks of heat injuries or mortalities (Urban et al., 2019) and deteriorated outdoor labor productivity (Liu et al., 2021; Parsons et al., 2022). However, our study shows that there may be a risk of overestimation in the heat stress index, attributable to the inappropriate assumptions of constant wind speed and solar radiation across time and space together with the insufficient understanding in sub-daily diurnal variation of the meteorological variables. Despite the fact that several physics-based heat stress indices (e.g., WBGT computed by Liljegren's model, Universal Thermal Climate Index) project an exacerbation of future heatwaves (e.g., Cardoso et al., 2023; García-León et al., 2021; Grundstein et al., 2013), sWBGT may

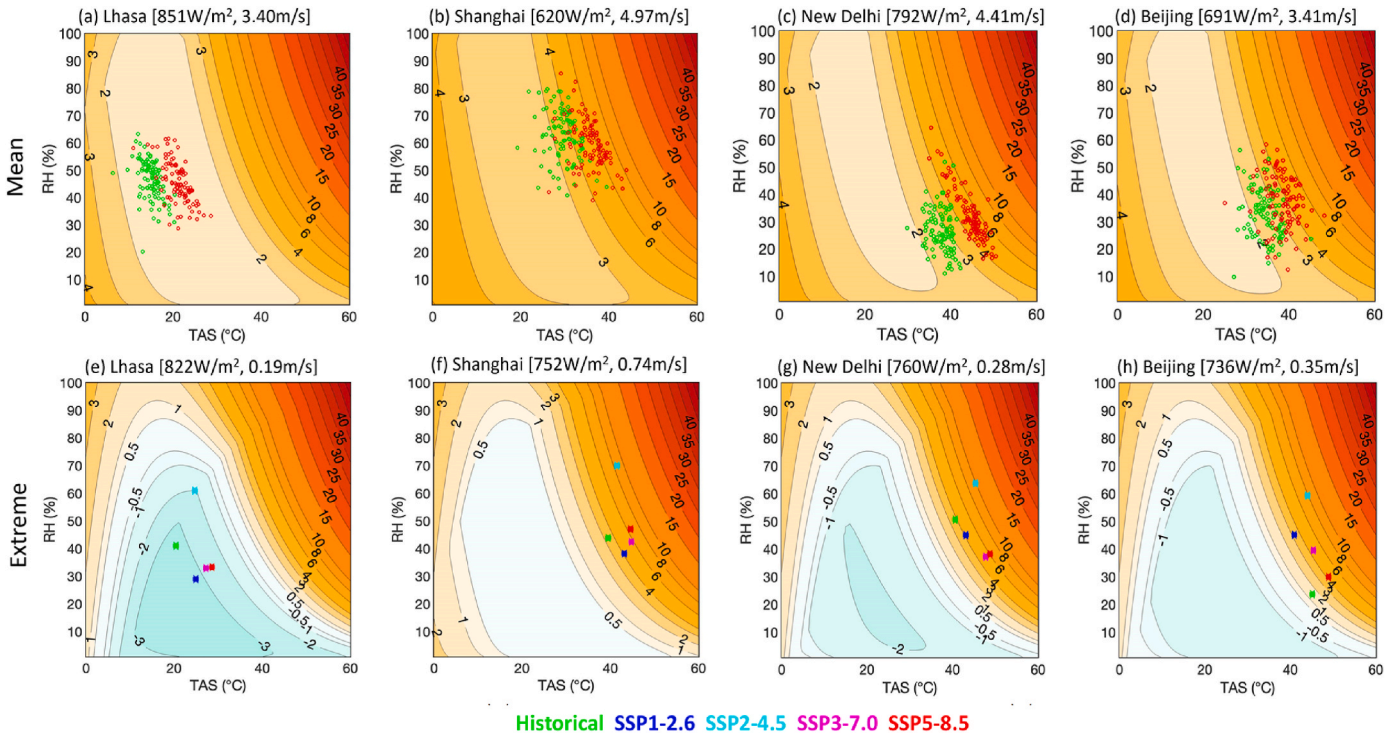

Fig. 6. The contour shading represents the bias of sWBGT (sWBGT-WBGT) under different combinations of TAS and RH, given fixed WS and RSDS levels representing the mean and extreme situation over grid points in Lhasa (29.75°N, 91.25°E), Shanghai (31.25°N, 121.50°E), New Delhi (28.50°N, 77.25°E), and Beijing (40.00 °N, 116.50°E), respectively. The dots on Fig. 6(a–d) represent the day when WBGT reaches the 0th (i.e., the minimum), 1st, 2nd, 3rd …, and 100th (i.e., the maximum) percentiles in the current (green) and future (red, SSP5-8.5) climates. Fig. 6(e–h) compares the 100th percentiles from all the emission scenarios. The result is first calculated for each model and the ensemble mean is presented. (For interpretation of the references to color in this figure legend, the reader is referred to the Web version of this article.)

Table 1
The spatial correlation between the bias of sWBGT's projected change in JJA mean with the JJA mean TAS, HURS, RSDS, WS during the historical period and with their change.

[sWBGT change – WBGT change]	Historical				Change			
	TAS	RH	RSDS	WS	TAS	RH	RSDS	WS
SSP1-2.6	0.83	0.39	0.06	0.37	−0.77	0.02	0.04	0.21
SSP2-4.5	0.84	0.41	0.08	0.34	−0.77	0.12	0.00	0.42
SSP3-7.0	0.84	0.42	0.09	0.38	−0.78	0.21	0.03	0.20
SSP5-8.5	0.83	0.44	0.10	0.38	−0.79	0.24	−0.02	0.29

provide a biased assessment that could trigger over-reacting alarms and negatively impact adaptation decisions. Therefore, our study emphasizes the importance of cautiously interpreting heat stress measured by sWBGT, especially over regions of hot, humid climate. Furthermore, the nonlinear sensitivity of WBGT to wind and solar radiation change in the extreme conditions (i.e., extreme low wind and/or high solar radiation) calls for more accurate, high spatiotemporal resolution climate projection data for providing a holistic view of the future heat that we will confront.

In conclusion, our findings highlight the limitations of using sWBGT as an ad hoc approximation for estimating outdoor heat stress levels and projecting future changes. Researchers and policymakers should exercise caution when using sWBGT and daily meteorological data as the bias may lead to an inaccurate understanding of the true impacts of heat stress on human health, labor productivity, and other climate-sensitive sectors. As the explicit calculation of Liljegren's model has recently been available in Python (Kong and Huber, 2022) and R (Casanueva et al., 2019), they are strongly recommended for use in combination with high-resolution climate data at sub-daily time scale for assessing outdoor heat stress in climate-change studies.

Nevertheless, several caveats of the current study should be noted. First, there exist a variety of formulas to simplify WBGT calculation, each with their pros and cons depending on their applications and assumptions. This study only assesses one formula that has been widely adopted. A more comprehensive assessment of other calculation methods would be a valuable and necessary future work to enhance our understanding of heat-stress assessments. In addition, this study takes the physics-based WBGT as a "ground truth" for counting the bias in sWBGT, yet it does not indicate that WBGT is a perfect index applicable for all outdoor heat stress assessments. Other outdoor heat stress indices (e.g., National Oceanic and Atmospheric Administration/National Weather Service heat index; Sylla et al., 2018) are also important, which take different assumptions regarding to human body's response to the ambient environment (Im et al., 2017b). Future heat stress studies may consider multiple heat stress indices for comprehensive assessments (Shin et al., 2022). Lastly, although Lilljegren's physics-based method has been widely recognized as the most accurate estimation of outdoor WBGT, more observations may be necessary for further validation and improvements in WBGT calculations, particularly for applications in specific location or workplace and for diverse populations.

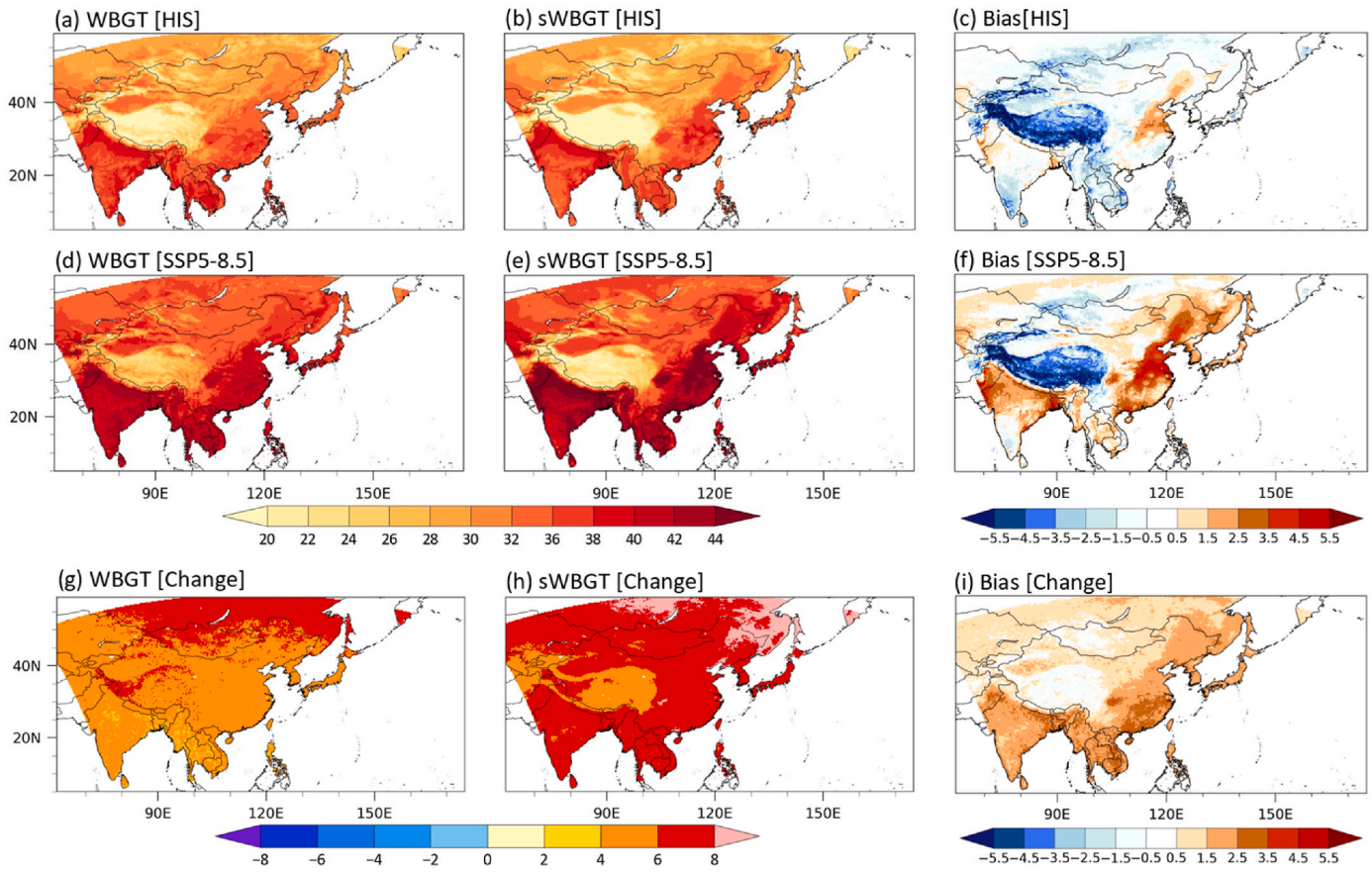

Fig. 7. The spatial distribution of the average intensity of heatwave events bias calculated using (a, d) WBGTmax and (b, e) sWBGTmax for the historical (1979–2014) and future (2065–2100, SSP5-8.5) periods. (c) and (f) are the bias of sWBGT during the two periods, respectively, and (g) and (h) are the projected change (2065–2100 vs. 1979–2014) using WBGT and sWBGT, respectively. (i) Is the bias of the projected change in sWBGT compared to WBGT. The unit is °C.

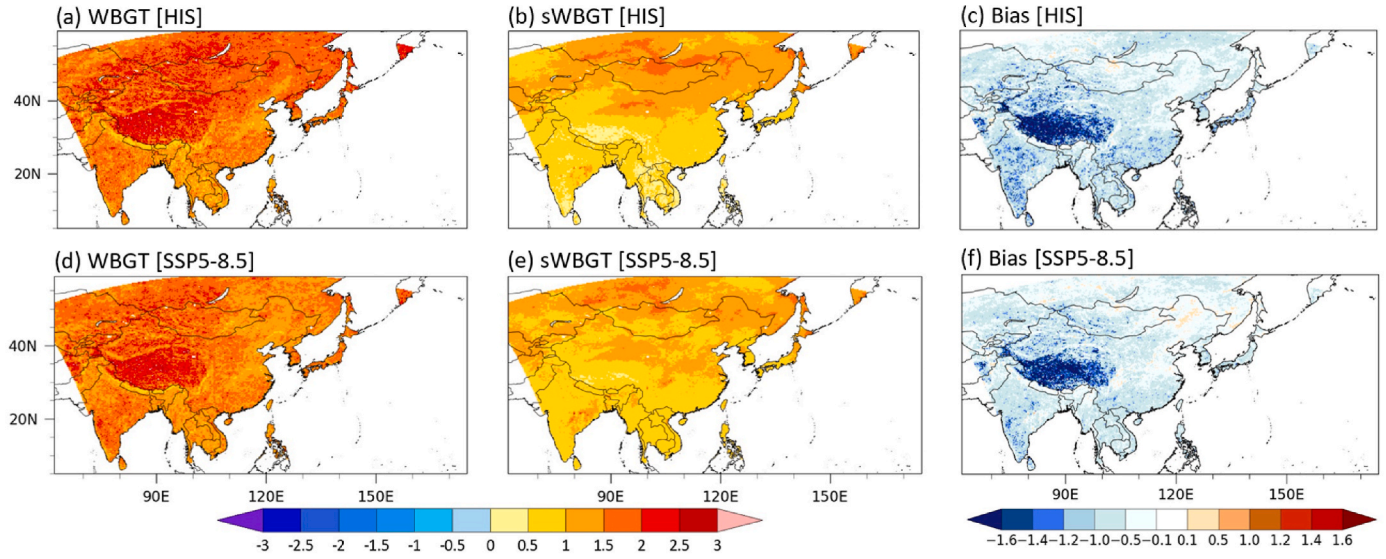

Fig. 8. The spatial distribution of the relative intensity (i.e., intensity - threshold) of heatwave events bias calculated using (a, d) WBGTmax and (b, e) sWBGTmax for the historical (1979–2014) and future (2065–2100, SSP5-8.5) periods. (c) and (f) are the bias of sWBGT during the two periods, respectively. The unit is °C.

Funding

This research was supported by the Korea Meteorological Administration Research and Development Program under grant No. KMI 2021-00912. Additionally, this research was partly supported by the Theme-based Research Scheme (T31-603/21-N) and General Research Fund (GRF16308722), which was funded by the Research Grants Council (RGC) of Hong Kong.

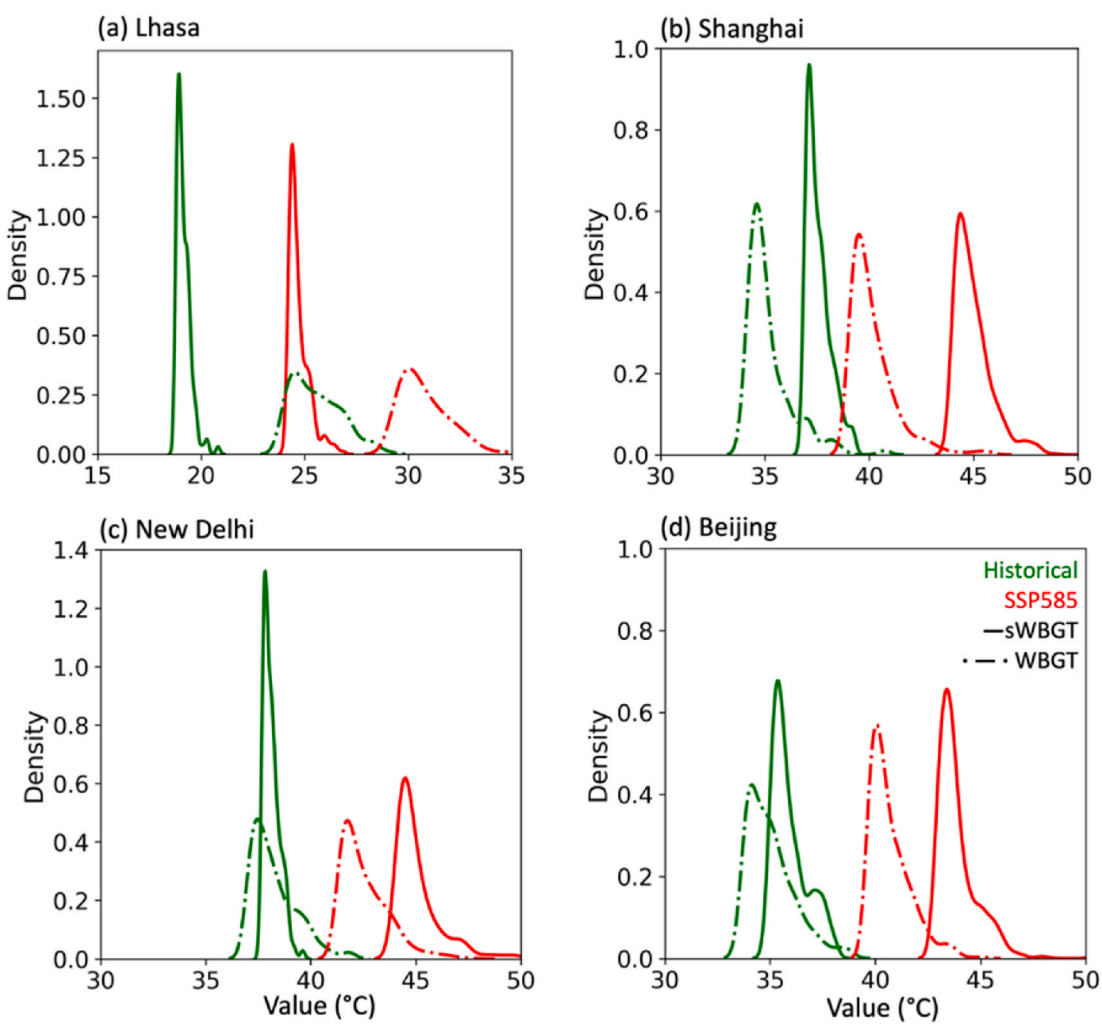

Fig. 9. The kernel density distribution estimated for extreme daily WBGTmax (dashed) and sWBGTmax (solid) (i.e., daily heat stress exceeding the 99th percentile of the period) during historical (1979–2014) and future (2065–2100, SSP5-8.5) periods. (a) to (d) is for the grid point selected from Lhasa (29.75°N, 91.25°E), Shanghai (31.25°N, 121.50°E), New Delhi (28.50°N, 77.25°E), and Beijing (40.00 °N, 116.50°E), respectively.

Data statement

The downscaled meteorological data over the CORDEX-East domain is archived in the institutional repository at https://doi.org/10.14711/dataset/GTXJVQ (Qiu et al., 2023). ERA5 data is downloaded from the Climate Data Store via https://doi.org/10.24381/cds.adbb2d47 (Hersbach et al., 2018). The WBGT is calculated using the python package provided by Kong and Huber (2022) at https://zenodo.org/record/5980536. R package "qmap" (https://CRAN.R-project.org/package = qmap; Gudmundsson, 2016) is used for applying QDM.

Data availability

Data will be made available on request.

CRediT authorship contribution statement

Liying Qiu: Conceptualization, Data curation, Formal analysis, Investigation, Methodology, Software, Validation, Visualization, Writing – original draft, Writing – review & editing. **Ziwei Zhu:** Data curation, Formal analysis, Investigation, Visualization. **Zixuan Zhou:** Writing – original draft, Writing – review & editing. **Eun-Soon Im:** Conceptualization, Methodology, Project administration, Supervision, Writing – review & editing. **Seung-Ki Min:** Project administration, Writing – review & editing. **Yeon-Hee Kim:** Data curation. **Yujin Kim:** Data curation. **Dong-Hyun Cha:** Data curation. **Joong-Bae Ahn:** Data curation. **Young-Hwa Byun:** Data curation.

Declaration of competing interest

The authors declare that they have no known competing financial interests or personal relationships that could have appeared to influence the work reported in this paper.

Acknowledgements

We would like to thank the two anonymous reviewers for their helpful and constructive feedback and suggestions. Also, we would for the open-source WBGT calculation code provided by Kong and Huber (2022), which were crucial for this work.

Appendix A. Supplementary data

Supplementary data to this article can be found online at https://doi.org/10.1016/j.wace.2024.100677.

References

American College of Sports Medicine (ACSM), 1984. Prevention of thermal injuries during distance running. Med. J. Aust. 141, 876–879. https://doi.org/10.5694/j.1326-5377.1984.tb132981.x.

Bai, L., Woodward, A., Cirendunzhu, Liu, Q., 2016. County-level heat vulnerability of urban and rural residents in Tibet, China. Environ. Health 15, 1–10. https://doi.org/10.1186/s12940-015-0081-0.

Becker, F.N., Fink, A.H., Bissolli, P., Pinto, J.G., 2022. Towards a more comprehensive assessment of the intensity of historical European heat waves (1979–2019). Atmos. Sci. Lett. 23, e1120 https://doi.org/10.1002/asl.1120.

Bumbaco, K.A., Dello, K.D., Bond, N.A., 2013. History of Pacific Northwest heat waves: synoptic pattern and trends. J. Appl. Meteorol. Climatol. 52, 1618–1631. https://doi.org/10.1175/JAMC-D-12-094.1.

Casanueva, A., Kotlarski, S., Herrera, S., Fischer, A.M., Kjellstrom, T., Schwierz, C., 2019. Climate projections of a multivariate heat stress index: the role of downscaling and bias correction. Geosci. Model Dev. (GMD) 12, 3419–3438. https://doi.org/10.5194/gmd-12-3419-2019.

Chen, X., Li, N., Liu, J., Zhang, Z., Liu, Y., Huang, C., 2020. Changes in global and regional characteristics of heat stress waves in the 21st century. Earth's Future 8, e2020EF001636. https://doi.org/10.1029/2020EF001636.

Dunne, J.P., Stouffer, R.J., John, J.G., 2013. Reductions in labour capacity from heat stress under climate warming. Nat. Clim. Change 3, 563–566. https://doi.org/10.1038/nclimate1827.

García-León, D., Casanueva, A., Standardi, G., Burgstall, A., Flouris, A.D., Nybo, L., 2021. Current and projected regional economic impacts of heatwaves in Europe. Nat. Commun. 12, 5807. https://doi.org/10.1038/s41467-021-26050-z.

Grundstein, A., Cooper, E., 2018. Assessment of the Australian Bureau of Meteorology wet bulb globe temperature model using weather station data. Int. J. Biometeorol. 62, 2205–2213. https://doi.org/10.1007/s00484-018-1624-1.

Grundstein, A., Elguindi, N., Cooper, E., Ferrara, M., 2013. Exceedance of wet bulb globe temperature safety thresholds in sports under a warming climate. Clim. Res. 58, 183–191. https://doi.org/10.3354/cr01199.

Hajat, S., Kovats, R.S., Atkinson, R.W., Haines, A., 2002. Impact of hot temperatures on death in London: a time series approach. J. Epidemiol. Community Health 56, 367–372. https://doi.org/10.1136/jech.56.5.367.

Hersbach, H., Bell, B., Berrisford, P., Hirahara, S., Horányi, A., Muñoz-Sabater, J., Nicolas, J., Peubey, C., Radu, R., Schepers, D., Simmons, A., Soci, C., Abdalla, S., Abellan, X., Balsamo, G., Bechtold, P., Biavati, G., Bidlot, J., Bonavita, M., De Chiara, G., Dahlgren, P., Dee, D., Diamantakis, M., Dragani, R., Flemming, J., Forbes, R., Fuentes, M., Geer, A., Haimberger, L., Healy, S., Hogan, R.J., Hólm, E., Janisková, M., Keeley, S., Laloyaux, P., Lopez, P., Lupu, C., Radnoti, G., de Rosnay, P., Rozum, I., Vamborg, F., Villaume, S., Thépaut, J.-N., 2020. The ERA5 global reanalysis. Q. J. R. Meteorol. Soc. 146, 1999–2049. https://doi.org/10.1002/qj.3803.

Im, E.-S., Choi, Y.W., Ahn, J.B., 2017. Worsening of heat stress due to global warming in South Korea based on multi-RCM ensemble projections. J. Geophys. Res. Atmos. 122 https://doi.org/10.1002/2017JD026731, 11,444–11,461.

Kjellstrom, T., Freyberg, C., Lemke, B., Otto, M., Briggs, D., 2018. Estimating population heat exposure and impacts on working people in conjunction with climate change. Int. J. Biometeorol. 62, 291–306. https://doi.org/10.1007/s00484-017-1407-0.

Kong, Q., Huber, M., 2022. Explicit calculations of wet-bulb globe temperature compared with approximations and why it matters for labor productivity. Earth's Future 10, e2021EF002334. https://doi.org/10.1029/2021EF002334.

Lee, D.-K., Cha, D.-H., 2020. Regional climate modeling for Asia. Geosci. Lett. 7, 13. https://doi.org/10.1186/s40562-020-00162-8.

Lee, S.-M., Min, S.-K., 2018. Heat stress changes over East Asia under 1.5° and 2.0°C global warming targets. J. Clim. 31, 2819–2831. https://doi.org/10.1175/JCLI-D-17-0449.1.

Lemke, B., Kjellstrom, T., 2012. Calculating workplace WBGT from meteorological data: a tool for climate change assessment. Ind. Health 50, 267–278. https://doi.org/10.2486/indhealth.ms1352.

Li, X.-X., 2020. Heat wave trends in Southeast Asia during 1979–2018: the impact of humidity. Sci. Total Environ. 721, 137664 https://doi.org/10.1016/j.scitotenv.2020.137664.

Liljegren, J.C., Carhart, R.A., Lawday, P., Tschopp, S., Sharp, R., 2008. Modeling the wet bulb globe temperature using standard meteorological measurements. J. Occup. Environ. Hyg. 5, 645–655. https://doi.org/10.1080/15459620802310770.

Lima, C.Z. de, Buzan, J.R., Moore, F.C., Baldos, U.L.C., Huber, M., Hertel, T.W., 2021. Heat stress on agricultural workers exacerbates crop impacts of climate change. Environ. Res. Lett. 16, 044020 https://doi.org/10.1088/1748-9326/abeb9f.

Liu, Y., Zhang, Z., Chen, X., Huang, C., Han, F., Li, N., 2021. Assessment of the regional and sectoral economic impacts of heat-related changes in labor productivity under climate change in China. Earth's Future 9, e2021EF002028. https://doi.org/10.1029/2021EF002028.

Parsons, L.A., Masuda, Y.J., Kroeger, T., Shindell, D., Wolff, N.H., Spector, J.T., 2022. Global labor loss due to humid heat exposure underestimated for outdoor workers. Environ. Res. Lett. 17, 014050 https://doi.org/10.1088/1748-9326/ac3dae.

Perkins, S.E., 2015. A review on the scientific understanding of heatwaves—their measurement, driving mechanisms, and changes at the global scale. Atmos. Res. 164, 242–267. https://doi.org/10.1186/s12992-023-00955-4.

Qiu, L., Im, E.-S., Min, S.-K., Kim, Y.-H., Cha, D.-H., Shin, S.-W., Ahn, J.-B., Chang, E.-C., Byun, Y.-H., 2023. Direct and indirect application of univariate and multivariate bias corrections on heat-stress indices based on multiple regional-climate-model simulations. Earth Syst. Dyn. 14, 507–517. https://doi.org/10.5194/esd-14-507-2023.

Russo, S., Sillmann, J., Sterl, A., 2017. Humid heat waves at different warming levels. Sci. Rep. 7, 7477. https://doi.org/10.1038/s41598-017-07536-7.

Shin, J.-Y., Kang, M., Kim, K.R., 2022. Outdoor thermal stress changes in South Korea: increasing inter-annual variability induced by different trends of heat and cold stresses. Sci. Total Environ. 805, 150132 https://doi.org/10.1016/j.scitotenv.2021.150132.

Spangler, K.R., Liang, S., Wellenius, G.A., 2022. Wet-bulb globe temperature, universal thermal climate index, and other heat metrics for US counties, 2000–2020. Sci. Data 9, 326. https://doi.org/10.1038/s41597-022-01405-3.

Sulikowska, A., Wypych, A., 2020. Summer temperature extremes in Europe: how does the definition affect the results? Theor. Appl. Climatol. 141, 19–30. https://doi.org/10.1007/s00704-020-03166-8.

Sylla, M.B., Faye, A., Giorgi, F., Diedhiou, A., Kunstmann, H., 2018. Projected heat stress under 1.5 °C and 2 °C global warming scenarios creates unprecedented discomfort for humans in West Africa. Earth's Future 6, 1029–1044. https://doi.org/10.1029/2018EF000873.

Takakura, J., Fujimori, S., Takahashi, K., Hasegawa, T., Honda, Y., Hanasaki, N., Hijioka, Y., Masui, T., 2018. Limited role of working time shift in offsetting the increasing occupational-health cost of heat exposure. Earth's Future 6, 1588–1602. https://doi.org/10.1029/2018EF000883.

Ullah, I., Saleem, F., Iyakaremye, V., Yin, J., Ma, X., Syed, S., Hina, S., Asfaw, T.G., Omer, A., 2022. Projected changes in socioeconomic exposure to heatwaves in South Asia under changing climate. Earth's Future 10, e2021EF002240. https://doi.org/10.1029/2021EF002240.

Urban, A., Hondula, D.M., Hanzlíková, H., Kyselý, J., 2019. The predictability of heat-related mortality in Prague, Czech Republic, during summer 2015—a comparison of selected thermal indices. Int. J. Biometeorol. 63, 535–548. https://doi.org/10.1007/s00484-019-01684-3.

Wei, J., Han, W., Wang, W., Zhang, L., Rajagopalan, B., 2023. Intensification of heatwaves in China in recent decades: roles of climate modes. npj Clim. Atmos. Sci. 6, 98. https://doi.org/10.1038/s41612-023-00428-w.

Xu, Z., FitzGerald, G., Guo, Y., Jalaludin, B., Tong, S., 2016. Impact of heatwave on mortality under different heatwave definitions: a systematic review and meta-analysis. Environ. Int. 89 (90), 193–203. https://doi.org/10.1016/j.envint.2016.02.007.